Journal of Applied Fluid Mechanics, Vol. 9, No.5, pp. 2435-2442, 2016.
Available online at www.jafmonline.net, ISSN 1735-3572, EISSN 1735-3645.
DOI:10.18869/acadpub.jafm.68.236.25356

Correlation-Based Transition Transport Modeling for Simulating Crossflow Instabilities

J. K. Xu†, J. Q. Bai, L. Qiao and Y. Zhang

School of Aeronautics, Northwestern Polytechnical University, Xi'an 710072, P. R. China

†*Corresponding Author Email: xujiakuanbond@163.com*

(Received July 24, 2015; accepted April 12, 2016)

ABSTRACT

A correlation-based transition model has been developed by Langtry and Menter for modern computational fluid dynamics codes, which is widely used for transition prediction in the field of turbomachinery and aircraft. Langtry's transition model could simulate bypass, laminar separation and streamwsie Tollmien–Schlichting wave transition. Even so, this model has no ability to predict the transition due to crossflow instabilities in three dimensional boundary layer. In this paper, a new correlation-based transport equation for the transition due to crossflow instabilities has been established based on the experiment data and self-similar equations. The new transport equation is introduced to describe the crosswise displacement thickness Reynolds number growth in boundary layer. This new equation is added to Langtry's intermittency factor equation to improve the ability of predicting transition. Finally, coupling of these transport equations and Shear Stress Transport (SST) turbulence model completes the new improved transition turbulence model. Comparisons of predictions using the new model with wind tunnel experiments of NLF (2)-0415 infinite swept wing and 6:1 inclined prolate spheroid validate the predictive qualities of the new correlation based transport equation.

Keywords: Turbulence; Laminar flow; Boundary layer transition; Transition model; Crossflow instabilities.

NOMENCLATURE

α	angle of attack	R_T	viscous ratio
C_f	skin friction coefficient	s	streamwise direction
C_p	pressure coefficient	Tu	freestream turbulence intensity
c	chord	u_i	cartesian velocity component
d	distance to nearest wall	x_i	cartesian coordinate
F_{length}	model-specific empirical function that controls transition length intermittency integral boundary-layer streamwise shape length of prolate spheroid Thwaites pressure gradient	β_H	hartree pressure gradient parameter
		δ_{CF}	crosswise displacement thickness
		μ	laminar kinematic viscosity
		μ_T	turbulent kinematic viscosity
		ρ	density
		Ω	vorticity magnitude
$Re_{\theta t}$	transition momentum thickness Reynolds number;	η	non-dimensional wall-normal distance in Falkner-Skan coordinate
$Re_{\delta CF}$	integral crosswise displacement thickness Reynolds number		

1. INTRODUCTION

Boundary layers transition plays an important role in the Computation Fluids Dynamics (CFD). Therefore, it is important to study the process of transition and develop the capability to predict transitional flow phenomena accurately. In Recent years, many methods were proposed to predict natural, bypass, separation-induced transition and crossflow instabilities induced transition. Such as the e^N method of Smith and Gamberoni (1956) and van Ingen (1956) which is a widely used method for transition prediction in applied aerodynamics; the laminar kinetic energy transition model of (Walters *et.al*. 2004, 2008, 2009) ; the transition closure model of (Hassan *et.al*. 1998; Robinson *et.al*. 1998); the important transition criterion of Arnal (Arnal 1992, 1994); the crossflow transition onset criteria of Medida (2013) which uses the modified crossflow Reynolds number and *k*-*ω*-γ turbulence

transition model of Wang & Fu (2012). These methods promote the development of transition prediction to some extent.

In this paper, the $\gamma-\overline{\mathrm{Re}_{\theta t}}$ correlation-based transition model proposed by (Langtry & Menter *et. al.* 2004-I, 2004-II 2009), is based on local variables, which could be calculated everywhere in the flow field. This transition model is an approach designed for modern CFD code and coupling with two transport equations, which lean on the structure of transport equations of two-equation turbulence models. One transport equation for the intermittency γ is built to trigger transition in the boundary layer and another one for the local momentum thickness Reynolds number control the onset location of transition (Seyfert *et al*. 2012). The transition transport model is coupled to the *k-ω* Shear Stress Transport (SST) turbulence model by Menter (1992). If the transition completed, the transition turbulence model would become original SST turbulence model. The correlation-based transition model has been used widely in many flow solvers. Currently, it can predict natural, bypass, and separation-induced transition. Since crossflow instabilities can cause earlier transition onset in 3-D boundary layers with yawed flow and favorable pressure gradients, it is essential for transition models to account for this important mechanism which usually occurred on the swept wings. In this paper, a new transport equation of crossflow displacement thickness Reynolds number which is a non-local variable, is established to predict crossflow instabilities induced transition in 3-D boundary layers based on experiment data.

2. NEW TRANSPORT EQUATION MODELING

2.1 Langtry and Menter's Transport Equation

The correlation-based transition transport equations of local momentum thickness Reynolds number and intermittency are formulated as follow:

$$\frac{\partial \overline{\mathrm{Re}_{\theta t}}}{\partial t}+u_i\frac{\partial \overline{\mathrm{Re}_{\theta t}}}{\partial x_i}=P_{\theta t}+\frac{1}{\rho}\frac{\partial}{\partial x_i}\left[\sigma_{\theta t}\left(\mu+\mu_t\right)\frac{\partial \overline{\mathrm{Re}_{\theta t}}}{\partial x_i}\right] \tag{1}$$

$$\frac{\partial \gamma}{\partial t}+u_i\frac{\partial \gamma}{\partial x_i}=P_\gamma-E_\gamma+\frac{1}{\rho}\frac{\partial}{\partial x_i}\left[\left(\mu+\frac{\mu_t}{\sigma_f}\right)\frac{\partial \gamma}{\partial x_i}\right] \tag{2}$$

Where $\sigma_{\theta t}=2.0$, $\sigma_f=1.0$, μ and μ_t are laminar dynamic viscosity value and eddy viscosity value respectively. The production source term $P_{\theta t}$ and P_γ, the destruction term of E_γ, are all described in Reference (Langtry & Menter 2009, Menter *et. al.* 2004) and need not be repeated here.

2.2 New Transport Equation for Crossflow Instabilities

Usually, the crosswise displacement thickness Reynolds number $\mathrm{Re}_{\delta CF}$ is chosen to be the characteristic parameter for crossflow instabilities induced transition (Arnal 1992) . The definition of non-local variable crosswise displacement thickness Reynolds number is expressed as

$$\mathrm{Re}_{\delta CF}=\frac{U_e\delta_{CF}}{\nu} \tag{3}$$

where U_e is the value of edge of velocity profiles, ν the laminar kinematic viscosity and the crosswise displacement thickness can be calculated by $\delta_{CF}=-\int_0^\delta\left(w/U_e\right)dy$. In the integral formula, w is the crosswise velocity. By solving Falkner Skan Cooke (FSC) self-similar equations (Cooke 1950) , a series velocity profiles were obtained at various pressure gradients and swept angles. For example, several non-dimensional velocity profiles at swept angle of30 degree were plotted in Fig. 1(a) and at swept angle of 45 degree were plotted in Fig. 1(b).

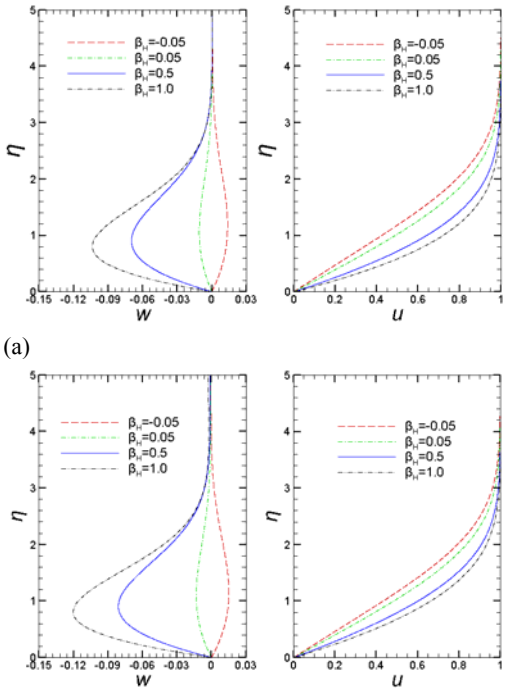

(a)

(b)

Fig. 1. FSC velocity profiles.

Based on the series velocity profiles, a lot of functions among shape factor H_{12} and crosswise displacement thickness $\mathrm{Re}_{\delta\mathrm{CF}}$ were completed. So the transport equation of crosswise displacement thickness Reynolds number $\mathrm{Re}_{\delta\mathrm{CF}}$ is proposed:

$$\frac{\partial \mathrm{Re}_{\delta\mathrm{CF}}}{\partial t}+\frac{\partial\left(U_j\,\mathrm{Re}_{\delta\mathrm{CF}}\right)}{\partial x_j}=P_{\delta\mathrm{CF}}+\frac{1}{\rho}\frac{\partial}{\partial x_j}\left[\frac{1}{\sigma_{\delta\mathrm{CF}}}\left(\mu+\mu_t\right)\frac{\partial \mathrm{Re}_{\delta\mathrm{CF}}}{\partial x_j}\right] \tag{4}$$

The source term of this equation is $P_{\delta CF}=f_k C_{R,CF}R_{I,CF}S$, where $\sigma_{\delta\mathrm{CF}}=1.0$, S is the

strain rate magnitude, $f_k = \exp\left[-(R_T/2.0)^{20}\right]$ the control function and $R_T = \mu_t/\mu$ the viscous ratio. The $C_{R,CF}$ function of source term $P_{\delta CF}$ is used to determine the unstable position and defined as

$$C_{R,CF} = 1 - \exp\left[-\left(\frac{\mathrm{Re}_{\mathrm{CF}}}{C_m(H_{12})\mathrm{Re}_{\mathrm{CF},0}}\right)^{C_z}\right] \quad (5)$$

In the formula, C_z = 8.0. The crossflow Reynolds number is $\mathrm{Re}_{\mathrm{CF}} = \frac{wd}{\nu}$ where w is the local crossflow velocity and d the minimum distance to the nearest wall. For swept wing, the crossflow velocity is calculated by the formula $w = U\sin\Delta$, the angle $\Delta = \Lambda_c - \Lambda + \Lambda_G$, where Λ_G is the geometry sweep angle, $\Lambda = \arctan\left(\tan(\Lambda_G)/\sqrt{1-C_p}\right)$ the local swept angle, and Λ_c is given by $\arctan(v/u)$. The variables u and v are Cartesian velocity components in the x- and z- directions respectively. Using this method, the crossflow velocity w could be calculated locally. If the configuration is complex, the redefined coordinate system method proposed by Choi *et al*. 2014 could be used here to calculate the new swept angle. Furthermore, to define the reference coordinate system, the external potential flow direction could be replaced with the local flow velocity, which could be adopted to estimate crossflow velocity w approximately. $\mathrm{Re}_{\mathrm{CF},0} = \frac{w_{\max}\delta_{10\%}}{\nu}$ is the critical crossflow Reynolds number proposed by Owen (1952) and has been modified in this paper to get a better result. In the definition, $w_{\max}$ is the maximum crossflow velocity and $\delta_{10\%}$ the larger boundary layer height where the crossflow velocity is 10% of its maximum value. The function $C_m(H_{12})$ was obtained by the FSC velocity profiles and expressed in eq. (7). Where C_{k1}=0.713; C_{k2}=-0.4598; C_{k3}=3.4824e-7; C_{k4}=4.152.

$$\mathrm{Re}_{\delta\mathrm{CF},0} = 235.1 + 18.9\cos(9.018H_{12}) + 37.38\sin(9.018H_{12}) + 7.57\cos(18.036H_{12}) + 5.129\cos(18.036H_{12}) \quad (6)$$

$$C_m(H_{12}) = \frac{(w\bullet d)_{\max}}{(w_{\max}\bullet\delta_{10\%})} = C_{k1}\exp(C_{k2}H_{12}) + C_{k3}\exp(C_{k4}H_{12}) \quad (7)$$

Another function $R_{I,CF}$ of source term $P_{\delta CF}$ is built to describe the growth rate of crosswise displacement thickness Reynolds number and defined as

$$R_{I,CF} = S(H_{12})D_{\mathrm{growth}}(H_{12}) \quad (8)$$

$S(H_{12})$ is the stream function and $D_{\mathrm{growth}}(H_{12})$ the development rate function which describes the development of crosswise displacement thickness Reynolds number along the streamwise direction. β_H is the Hartree pressure gradient parameter defined in Falkner-Skan-Cooke equations.

$$S(H_{12}) = \begin{cases} \left|(81.98H_{12}^3 - 649.6H_{12}^2 + 1710H_{12} - 1465)(H_{12} - 2.59)\right| & H_{12} < 2.59 \\ \left|(96.44H_{12}^3 - 764.2H_{12}^2 + 2012H_{12} - 1724)(H_{12} - 2.59)\right| & H_{12} \geq 2.59 \end{cases} \quad (9)$$

$$D_{\mathrm{growth}}(H_{12}) = -1.21\beta_H^5 + 2.711\beta_H^4 - 2.036\beta_H^3 + 0.5214\beta_H^2 + 0.07126\beta_H + 0.4031 \quad (10)$$

2.3 Implementation into Intermittency Equation

There were still some parameters unknown to solve the new transport equation. The Hartree pressure gradient parameter β_{H} and streamwise shape factor H_{12} need to be calculated. As the Thwaites pressure gradient factor $\lambda_\theta \equiv \frac{\theta^2}{\nu}\frac{dU}{ds}$, the Hartree pressure gradient parameter β_{H} could be computed by the formula as follow:

$$\frac{\lambda_\theta}{\beta_{\mathrm{H}}} = \left(\int_0^\delta \frac{u}{U_e}\left(1 - \frac{u}{U_e}\right)d\eta\right)^2 \quad (11)$$

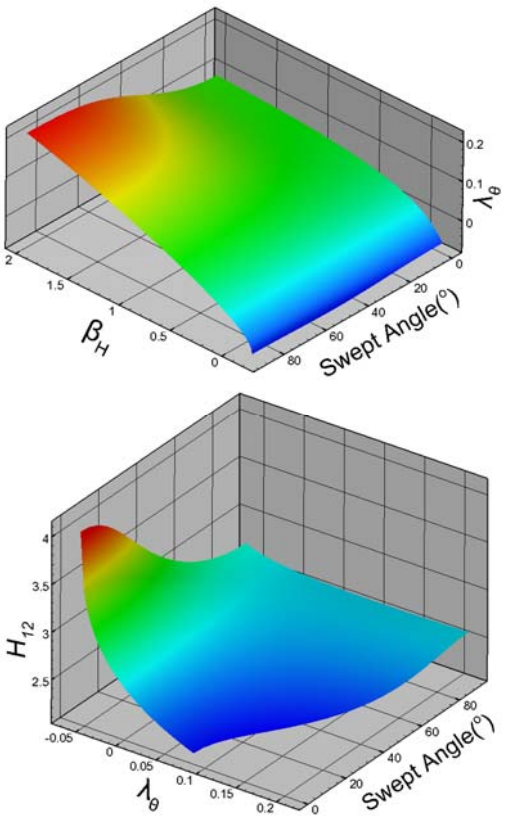

Fig. 2. The relationship among Hartree pressure gradient factor, shape factor and Thwaites pressure gradient factor.

Here, it can be observed that Thwaites pressure

gradient parameter λ_θ , is a function of the Hartree parameter β_H, and the local sweep angle Λ . Meanwhile, it is also a function of the shape factor H_{12} and the local sweep angle Λ :

$$\lambda_\theta = f(\beta_H, \Lambda) \quad \lambda_\theta = f(H_{12}, \Lambda) \tag{12}$$

The functions could be obtained by solving FSC equations as shown in Fig. 2. For another parameter, the local swept angle Λ can be calculated using the method proposed by Hogberg (1998) who assumes that there is no pressure gradient in the spanwise direction. So the local swept angle is the intersection angle between the pressure gradient direction and the local flow velocity direction.

For the onset Reynolds number based on the crosswise displacement thickness, the C1 criterion proposed by Ainal is chosen to judge the transition due to crossflow instability. For this purpose, the C1-criterion of Arnal (1992) is adopted as follows:

$$\begin{aligned} &\mathrm{Re}_{\delta CF,Exp} = \frac{300}{\pi}\arctan\left(\frac{0.106}{(H_{12}-2.3)^{2.05}}\right) && 2.3 \le H_{12} < 2.7 \\ &\mathrm{Re}_{\delta CF,Exp} = 150.0, && H_{12} < 2.3 \end{aligned} \tag{13}$$

Hence, the transition onset function is changed:

$$\begin{aligned} &\mathrm{F}_{onset4} = \mathrm{Re}_{\delta CF} / \mathrm{Re}_{\delta CF,Exp}; \\ &\mathrm{F}_{onset1} = \max\left(\mathrm{F}_{onset1\_original}, \mathrm{F}_{onset4}\right) \end{aligned} \tag{14}$$

where $\mathrm{F}_{onset1\_original}$ is the original transition onset function in the Langtry's $\gamma - \overline{\mathrm{Re}_{\theta t}}$ transition model, which accounts for the two-dimensional transition phenomena. F_{onset4} is a corresponding function introduced to account for three-dimensional crossflow-induced transition.

The F_{length} function is an empirical correlation that controls the length of the transition region, and the value should be calibrated when transition due to crossflow instability becomes dominant. Through the efforts, the new correlation for crossflow instabilities transition is expressed in eq. (15)

$$\mathrm{F}_{length,CF} = C_{L,4}\frac{C_{L,1} + \left(\frac{\overline{\mathrm{Re}_{\delta CF}}}{C_{L,2}}\right)^4}{C_{L,3} + \left(\frac{\overline{\mathrm{Re}_{\delta CF}}}{C_{L,2}}\right)^4} \tag{15}$$

Where $C_{L,1} = 117.3; C_{L,2} = 21.6; C_{L,3} = 1.0; C_{L,4} = 0.3$.

And the length function function will be used when the crossflow instabilities dominates. Through the new onset function and new length function, the new transport equation is implemented into the intermittency equation. Finally, the present transition model has been calibrated for use with the SST turbulence model Menter (1994). The coupling between the transition model and the turbulence model had no dif-ference with that way of Langtry (2009).

3. RESULTS AND DISCUSSIONS

In the present work, an in-house structured Reynolds averaged Navier–Stokes solver is used as the baseline flow solver. The solver is capable of analyzing two and three dimensional configurations in either time accurate or steady-state (non-time-accurate) simulations using a variety of discretization schemes and time-marching algorithms. The spatial discretization involves a semi-discrete finite-volume approach. Upwind-biasing is used for the convective and pressure terms, while central differencing is used for the shear stress and heat transfer terms. Time advancement is implicit with the ability to solve steady or unsteady flows. Multi-grid and mesh sequencing are available for convergence acceleration with the MPI (Message Passing Inteface) parallelization computation. In this work, all of the transition prediction results are obtained by using the new correlation-based transition transport equations coupling with the SST turbulence model.

3.1 Validation Test Case 1: NLF (2)-0415 Infinite Swept Wing

The new correlation-based transition transport equation is applied to the NLF (2)-0415 infinite swept wing which has been designed in order to investigate transition due to crossflow instabilities. This experiments were conducted in the wind tunnel at Arizona State University (Dagenhart and Saric 1999)**.** The freestream turbulence intensity of the wind tunnel was about 0.09%. In the process of numerical solving, the ambient source term was introduced to keep the turbulence intensity in the front of the wing. The Reynolds number of infinite swept wing experiments varies from 1.9×10^6 to 3.72×10^6 and the angle of attack is -4 degree for all transition related experiments. The transition locations was measured with naphthalene flow visualization technique, hot wire, and hot film measurements. Once the Reynolds number greater than 2.3×10^6, the transition process was almost dominated by crossflow instabilities. If the Langtry's correlation-based transition transport equation was used here, there would be a large difference of transition locations between the experiment data and CFD predictions. The number of grid elements in the wall-normal direction is 61; the chordwise resolution is 121 cells on either wing side. Here, $y^+(1)$ of the cell next to the wall is smaller than 1.0.

To compare with experiment, transition onset was selected to be the point where γ_{eff} = 0.5.Then the results of the computations comparing with the experiment data are plotted in Fig.3. The transition locations are shown depending on the Reynolds number. Computations were performed with the Langtry's correlation-based transition model and the present new correlation-based transition model. In the Fig.3, it can be seen that the results of the present equations are in very good agreement with the experimental data. All the computed transition location is close to the experimental area given by a

naphthalene technique measurement. Furthermore, compared to the Langtry's transition model which almost became invalid at Reynolds number of 3.72 $\times 10^6$, the result of new correlation-based transition model proposed in this paper is very promising as shown in Fig.4. For details, Fig 5 shows the pressure coefficient and skin friction coefficient around the upper surface of NLF (2)-0415 infinite swept wing at the Reynolds number of 3.72×10^6 and Mach number of 0.2384. It can be seen from the figure that, the transition occurred near the 27%c position where skin friction coefficient growths spurt. Fig.6 and Fig.7 show the contour of crosswise displacement thickness Reynolds number and effective intermittency around the NLF (2)-0415 infinite swept wing at the Reynolds number of 3.72×10^6.

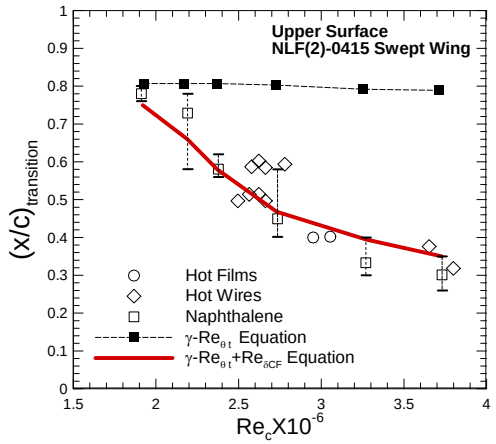

Fig. 3. Transition locations on the upper surface of NLF (2)-0415 wing.

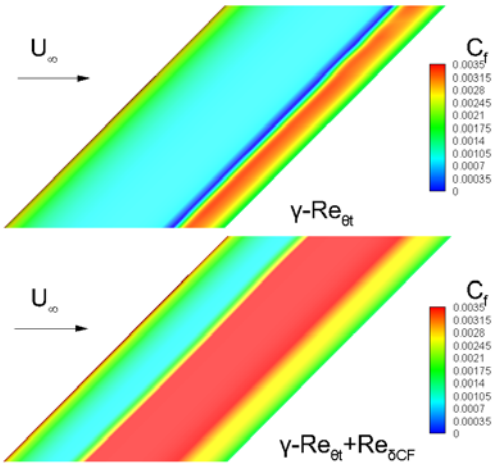

Fig. 4. The comparison of skin friction coefficient results between γ-Reθt model and new γ-Reθt-ReδCF model.

3.2 Validation Test Case 2: Inclined Prolate Spheroid

The second case for validation is the inclined 6:1 prolate spheroid, which contains complex flow phenomenon of boundary layer flows. The experiment was conducted in the low speed wind tunnel by Kreplin *et.al*. and the experimental data could be found in a lot of researcher's papers (Meier *et.al.* 1980; Choi *et.al*. 2014; Kreplin *et.al*. 1985; Krimmelbein *et.al.* 2010). The length of the spheroid L=2.4m. The experiment case of the inclined 6:1 prolate spheroid at three Reynolds numbers of 3.01×10^6, 4.48×10^6, 8.52×10^6 and the same angle of attack of 29.5 degree were selected for transition simulation. Before that, calculations at Reynolds number of 7.2×10^6 and angle of attack of 30 degree were conducted to compare with the experiment data. Langtry's $\gamma-\overline{\mathrm{Re}_{\theta t}}$ correlation-based transition model and the new $\gamma-\overline{\mathrm{Re}_{\theta t}}-\mathrm{Re}_{\delta CF}$ correlation-based transition model proposed in this paper were both used to predict the transition for those cases. The free stream turbulence intensity and the viscosity ratio were set as 0.1% and 10.0 respectively for the calculation. The number of grid elements in the wall-normal direction is 81 so that $y^+(1)$ of the cell next to the wall is smaller than 1.0.

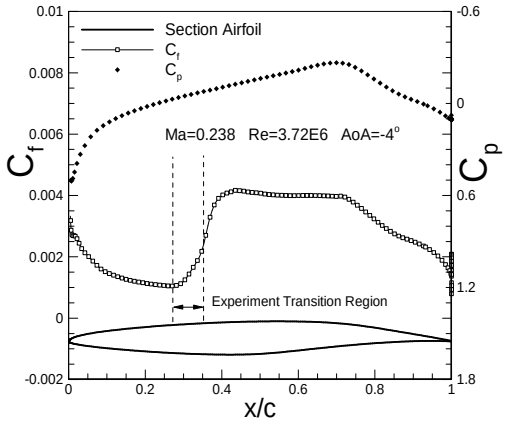

Fig. 5. The comparison of pressure coefficient and skin friction coefficient on the upper surface between experiment data and calculation result of new γ-Reθt-ReδCF model.

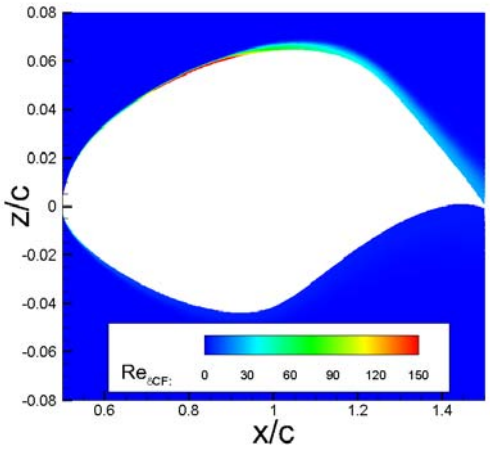

Fig. 6. The contour of crosswise displacement thickness Reynolds number distribution around NLF (2)-0415 infinite swept wing.

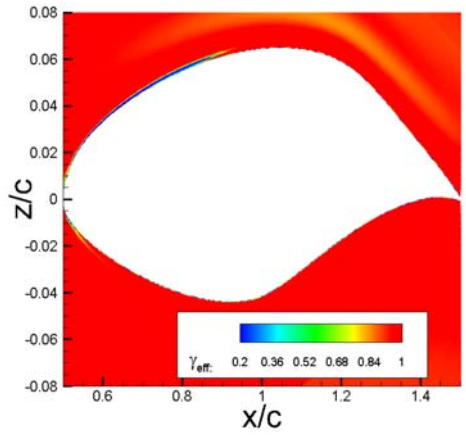

Fig. 7. The contour of effective intermittency around NLF (2)-0415 infinite swept wing.

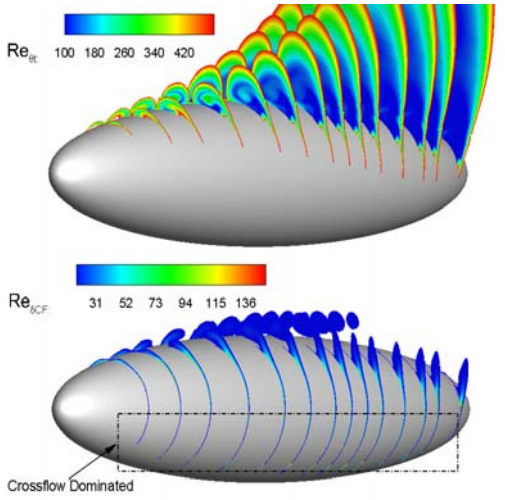

Fig. 8. Computed contours of transport Reynolds numbers in the present transition model at Re=7.2×10^6 and angle of attack of 30 degree.

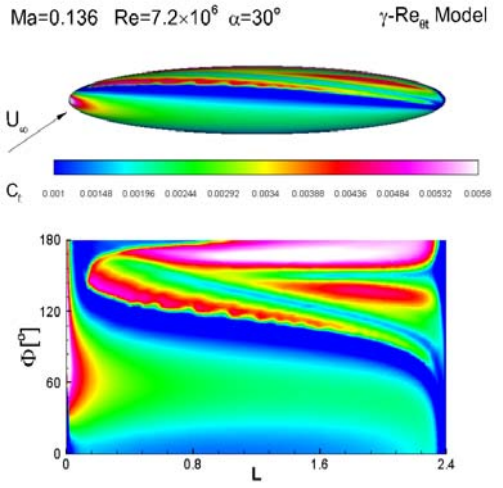

(a) Langtry and Menter's model

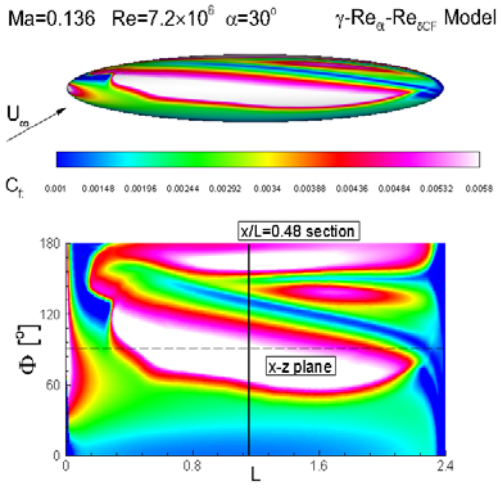

(b) Present model

Fig. 9. Comparison of skin friction coefficient contours on 6:1 prolate spheroid at Re = 7.2×10^6 and angle of attack of 30 degree.

Firstly, Fig.8 shows the distributions of local transition mo-mentum thickness Reynolds number and the local cross-wise displacement thickness Reynolds number around the prolate spheroid. The contour of skin friction coefficient was calculated by $\gamma-\overline{\mathrm{Re}_{\theta t}}$ transition model and the new transition model and shown in Fig.9 at Reynolds number of 7.2×10^6 and angle of attack of 30 degree.

Further analyzing, the skin friction coefficient distribution obtained by these two transition models at the central x-z cutting plane and x/L=0.48 section of the prolate spheroid are plotted in Fig.10 to compare with the experiment data. For the Reynolds number of 7.2×10^6, Langtry's $\gamma-\overline{\mathrm{Re}_{\theta t}}$ correlation-based transition model is invalid for the transition due to crossflow instabilities. It is obvious that the new model could capture the crossflow instabilities induced transition, laminar separation bubble induced transition, turbulent separation and attachment better.

In Fig.11, the predicted skin friction distributions on the prolate spheroid surface are shown using the new transition model for comparing with experiment data. In the case of Re = 3.01×10^6, TS waves is dominant to control the transition. With the Reynolds number increasing, the crossflow instabilities dominate gradually. At Re = 4.48×10^6, crossflow instabilities trigger the transition in the middle of the prolate spheroid. Also the crossflow instabilities become stronger as Reynolds number increasing to Re = 8.52×10^6. Above all, the new correlation-based transition model proposed in this paper could not only simulates the streamwise transition phenomenon but also captures the transition due to crossflow instabilities. In conclusion, the measured and predicted transition locations by using original $\gamma-\overline{\mathrm{Re}_{\theta t}}$ model and present model on the prolate spheroid are plotted and compared in Fig. 12(a) and Fig. 12(b) at various Reynolds number. All the data calculated by the new transition model for transition due to crossflow instabilities are in good agreement with experiment data.

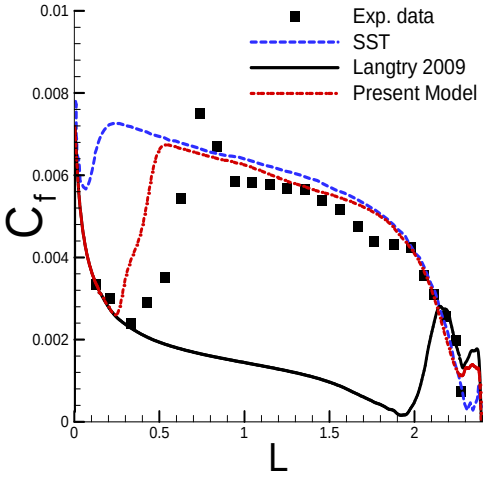

(a)

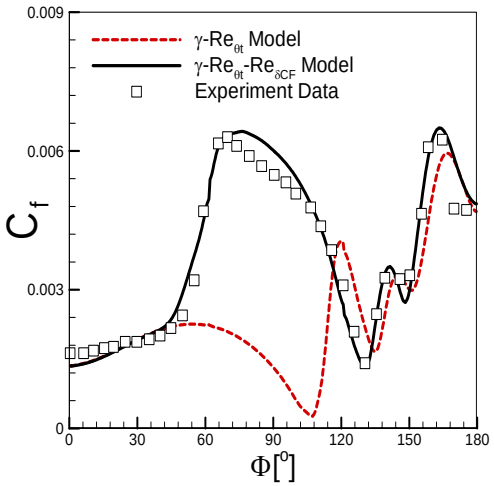

(b)

Fig. 10. Skin friction coefficient lines along the x-z cutting plane (a) and x/L=0.48 section (b) on 6:1 prolate spheroid at Re = 7.2×10^6 and angle of attack of 30 degree.

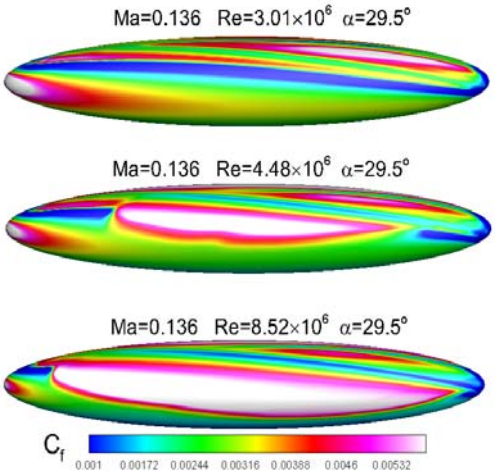

Fig. 11. Skin friction coefficient contours on 6:1 prolate spheroid at angle of attack of 29.5 degree and three Reynolds numbers (a) Re = 3.01×10^6 , (b) Re = 4.48×10^6 , and (c) Re = 8.52×10^6.

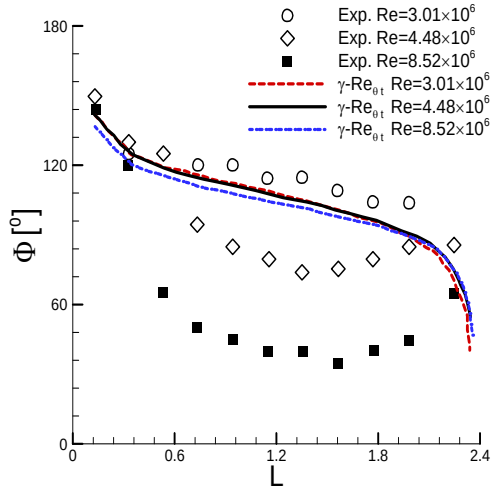

(a)

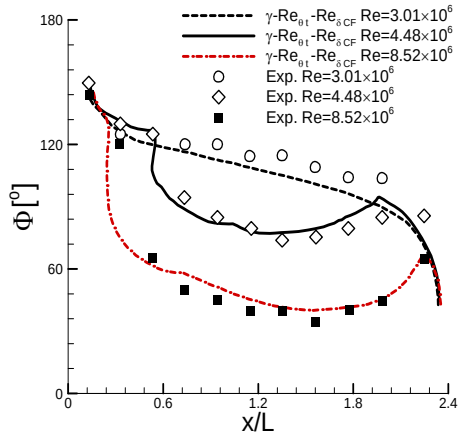

(b)

Fig. 12. Comparison of experimental data and predicted transition locations on 6:1 spheroid at angle of attack of 29.5 degree.

4. CONCLUSIONS

A new correlation-based transition transport equation for crossflow transition has been developed and applied to the SST turbulence model. The application of the new transport equation to the infinite swept NLF (2)-0415 wing and the 6:1 inclined prolate spheroid show very promising results compared with experiment data. The new model could predict the corssflow transition well for the incompressible boundary layer, it would be enhanced for compressible boundary layer in the future.

ACKNOWLEDGEMENTS

This work was supported by the National Basic Research Program of China (No. 2014CB744804).

REFERENCES

Arnal, D. (1992). Boundary Layer Transition: Prediction, Application to Drag Reduction,

AGARD Report 786, March 1992.

Arnal, D. (1994). Boundary Layer Transition: Predictions Based on Linear Theory. *AGARD Report 793, April 1994.*

Choi J. H. and Kwon O. J. (2014). Enhancement of a Correlation-Based Transition Turbulence Model for Simulating Crossflow Instability. *AIAA SciTech. January 2014. AIAA paper: 2014-1133.*

Cooke J. C. (1950). The Boundary Layer of a Class Of Infinite Yawed Cylinders, *Mathematical Proceedings of the Cambridge Philosophical Society*, Vol. 46, No. 4, 1950, pp. 645–648.

Dagenhart J. R. and W. S. Saric (1999). Crossflow Stability and Transition Experiments in Swept-Wing Flow. *NASA Langley Research Center TP-1999-209344*, Hampton, USA.

Hogberg, M. and D. Henningson (1998). Secondary Instability of Cross-Flow Vortices in Falkner-Skan-Cooke Boundary Layers. *Journal of Fluid Mechanics* 368, 339-357.

Kreplin, H. P., H. Vollmers and H. U. Meier (2009). Wall Shear Stress Measurements on an Inclined Prolate Spheroid in the DFVLR 3M×3M Low Speed Wind Tunnel. *Göttingen, DFVLR-AVA, Rept. IB 222-84 A 33, Göttingen, Germany 1985.*

Krimmelbein, N. and A. Krumbein (2010). Automatic Transition Prediction for Three-Dimensional Configurations with Focus on Industrial Application. 40th Fluid Dynamics Conference. *AIAA paper* 2010-4292.

Langtry, R. B. and F. R. Menter (2009). Correlation-Based Transition Modeling for Unstructured Parallelized Computational Fluid Dynamics Codes. *AIAA Journal* 47(12), 2894–2906.

Medida, S. and J. D. Baeder (2013). A New Crossflow Transition Onset Criterion for RANS Turbulence Models. *AIAA Paper* 2013-3081.

Meier, H. U. and H. P. Kreplin (1980). Experimental Investigation of the Boundary Layer Transition and Separation on a Body of Revolution. *Zeitschrift fuer Flugwissenschaften und Weltraumforschung* 4, 65-71.

Menter, F. R. (1992). Two-Equation Eddy-Viscosity Turbulence Models for Engineering Applications. *AIAA Journal* 32(8), 1598–1605.

Menter F. R., R. B. Langtry and S. R. Likki (2004). A Correlation-Based Transition Model Using Local Variables Part I: Model Formulation. *Journal of Turbomachinery* 128(3), 413–422.

Menter, F. R., R. B. Langtry and S. R. Likki (2004). A Correlation-Based Transition Model Using Local Variables Part II: Model Formulation. *Journal of Turbomachinery* 128(3), 423–434.

Owen, P. R. and D. J. Randall (2009). Boundary-layer transition on a swept-back wing. *R. A. E. TM Aero 277, 1952.*

Robinson, D. F. and H. A. Hassan (1998). Further Development of the k–ζ (Enstrophy) Turbulence Closure Model. AIAA Journal 36, (10), 1825–1833.

Seyfert, C. and A. Krumbein (2012). Evaluation of a Correlation-Based Transition Model and Comparison with the eN Method. *Journal of Aircraft* 49(6), 1765-1773.

Smith, A. M. O. and N. Gamberoni (1950). Transition, Pressure Gradient and Stability Theory, *Douglas Aircraft Company. Rept*. ES-26388, Long Beach, CA, 1956.

van Ingen, J. L. (1956). A Suggested Semi-Empirical Method for the Calculation of the Boundary Layer Transition Region, *Delft University of Technology. Rept*. VTH-74, Delft, The Netherlands.

Walters, D. K. (2009). Physical Interpretation of Transition-Sensitive RANS Models Employing the Laminar Kinetic Energy Concept. *ERCOFTAC Bulletin* 80, 67-71.

Walters, D. K. and D. Cokljat (2008). A Three Equation Eddy Viscosity Model for Reynolds Averaged Navier Stokes Simulations of Transitional Flow. *Journal of Fluids Engineering* 130(12), 121401.

Walters, D. K. and H. L. James (2004). A New Model for Boundary Layer Transition Using a Single-Point RANS Approach. *Journal of Turbomachinery* 126(1), 193-202.

Wang, L. and S. Fu (2012). A modular RANS approach for modelling laminar–turbulent transition in turbomachinery flows. *International Journal of Heat and Fluid Flow* 34(2012), 62-69.

Warren, E. S. and H. A. Hassan (1998). Transition Closure Model for Predicting Transition Onset. *Journal of Aircraft* 35(5), 769–775.